Research article

Journal of MASS SPECTROMETRY

Received: 4 August 2013 Revised: 6 September 2013 Accepted: 6 September 2013 Published online in Wiley Online Library

(wileyonlinelibrary.com) DOI 10.1002/jms.3281

Z-sinapinic acid: the change of the stereochemistry of cinnamic acids as rational synthesis of a new matrix for carbohydrate MALDI-MS analysis

María L. Salum, Lucia M. Itovich and Rosa Erra-Balsells*

Successful application of matrix-assisted laser desorption/ionization (MALDI) MS started with the introduction of efficient matrices such as cinnamic acid derivatives (i.e. 3,5-dimethoxy-4-hydroxycinnamic acid, SA; α-cyano-4-hydroxycinnamic acid). Since the empirical founding of these matrices, other commercial available cinnamic acids with different nature and location of substituents at benzene ring were attempted. Rational design and synthesis of new cinnamic acids have been recently described too. Because the presence of a rigid double bond in its molecule structure, cinnamic acids can exist as two different geometric isomers, the *E*-form and *Z*-form. Commercial available cinnamic acids currently used as matrices are the geometric isomers *trans* or *E* (*E*-cinnamic and *trans*-cinnamic acids). As a new rational design of MALDI matrices, *Z*-cinnamic acids were synthesized, and their properties as matrices were studied. Their performance was compared with that of the corresponding *E*-isomer and classical crystalline matrices (3,5-dihydroxybenzoic acid; norharmane) in the analysis of neutral/sulfated carbohydrates. Herein, we demonstrate the outstanding performance for *Z*-SA. Sulfated oligosaccharides were detected in negative ion mode, and the dissociation of sulfate groups was almost suppressed. Additionally, to better understand the quite different performance of each geometric isomer as matrix, the physical and morphological properties as well as the photochemical stability in solid state were studied. The influence of the *E*/*Z* photoisomerization of the matrix during MALDI was evaluated. Finally, molecular modeling (density functional theory study) of the optimized geometry and stereochemistry of *E*-cinnamic and *Z*-cinnamic acids revealed some factors governing the analyte–matrix interaction. Copyright © 2013 John Wiley & Sons, Ltd.

Additional supporting information may be found in the online version of this article at the publisher's web site.

Keywords: neutral carbohydrates; sulfated carbohydrates; *Z*-sinapinic acid; *Z*-ferulic acid; *Z*-coumaric acid; *E*-sinapinic acid; *E*-ferulic acid; *E*-coumaric acid

Introduction

Since their introduction as matrices at the beginning of ultraviolet matrix-assisted laser desorption/ionization (LDI) mass spectrometry (MALDI-MS) development, cinnamic acid derivatives, particularly 3,5-dimethoxy-4-hydroxycinnamic acid [sinapinic acid (SA)][1] and α-cyano-4-hydroxycinnamic acid (CHCA),[2] have been extensively used especially for protein and peptide analysis. Since the early times, other commercial available cinnamic acids were used for proteins[1] and oligodeoxyribonucleotides.[3] As CHCA and SA have been successfully used, efforts to prepare new compounds rationally designed, keeping the cinnamic basic structure, have been made. Thus, the synthesis and applications of α-cyano-4-chlorocinnamic acid (Cl-CHCA),[4] (E)-2-cyano-3-(naphthalene-2-yl) acrylic acid[5] and (2E)—3-(anthracen-9-yl)-2-cyanoprop-2enoic acid[5] have been recently described. It is important to point out that the cinnamic acids used as matrices are the geometric isomers *trans or E* (*E*-cinnamic and *trans*-cinnamic acids; Scheme 1), and although, sometimes this fact is not specified, it is an important point to take into account. Cinnamic acids can exist in geometric forms *E* and *Z*.[6] Both exist in nature, especially in plants.[7] Photochemical *E*-*Z* isomerization of alkenes is a well known one-step process (Scheme S1(a)).[8] It is a special tool for synthesis in preparative organic photochemistry.[8–10] It has a key role in many photobiological phenomena[8–10] and technological applications.[11,12] It has been described in gas, liquid and in solid state.[8–15]

Although the extensive studies of *E*-cinnamic acids as matrices, *Z*-cinnamic acids were never tested in MALDI-MS experiments. Recently, we described a highly efficient one-pot preparation of *Z*-cinnamic acids by *E*-*Z* photoisomerization.[16,17] Thus, having at hand pure *Z*-cinnamic acids, we studied their behavior as MALDI matrices for carbohydrate analysis and compared with that of the corresponding *E*-isomer. This is the first attempt to check *Z*-isomers as matrices.

In the present paper, neutral and sulfated carbohydrates were chosen as analytes because we are interested in the development of new matrices for sugar analysis.[18,19] As it is known, classic MALDI cinnamic acid matrices [i.e. *E*-SA[20,21]; *E*-3-methoxy-4-hydroxycinnamic acid, *E*-ferulic acid (*E*-FA)[20]] do not perform well in carbohydrate analysis.[22] MALDI-MS analysis of sulfated

* *Correspondence to: Rosa Erra-Balsells, CIHIDECAR-Departamento de Química Orgánica, FCEN, Universidad de Buenos Aires, Pabellón II, 3er P, Ciudad Universitaria, 1428 Buenos Aires, Argentina. E-mail: erra@qo.fcen.uba.ar*

CIHIDECAR-Departamento de Química Orgánica, FCEN, Universidad de Buenos Aires, Pabellón II, 3er P, Ciudad Universitaria 1428 Buenos Aires, Argentina

Journal of MASS SPECTROMETRY

Scheme 1. General structure of geometric isomers of an alkene: i.e. in the case of cinnamic acids A corresponds to the aryl group (Ar) and B to the –COOH group.

oligosaccharides is problematic because labile sulfate groups are frequently dissociated [in-source decomposition (ISD)], and thus ion species of intact molecules are hardly detected.[22,23] Among commercial cinnamics, *E*-SA was checked for sulfated carbohydrates, but the presence of abundant matrix ions in the region of the molecular ion interfered with the detection.[21] Methods such as stabilizing by derivatization of sulfate groups[22,23] and development of cool matrices such as 2,5-dihydroxybenzoic acid [gentisic acid (GA)] and ionic liquid matrices[23,24] have been reported. GA is a cool matrix widely used for carbohydrate analysis. A weak point of GA is the formation of inhomogeneous needle-shaped crystals, and therefore, the analytes are ionized in only a few small areas on the probe called sweet spots. On the contrary, *nor*-harmane (nHo) as matrix provides abundant homogeneously distributed sweet spots all over the sample but behaves as a hotter matrix than GA in similar experiments.[25]

In the present paper, we studied and compared the *E*-forms and *Z*-forms of SA, FA and coumaric acid (CuA) as matrices for carbohydrate analysis. GA and nHo were used as reference matrices. For the description of the results, we focused our attention on *E*-SA and *Z*-SA. Physical and morphological properties of both isomers as well as the photochemical stability in solid state were compared too. Molecular modeling of the optimized geometry and stereochemistry of *E*-cinnamic and *Z*-cinnamic acids (i.e. *E*-SA and *Z*-SA), in the framework of density functional theory at the unrestricted Becke, three-parameter, Lee-Yang-Parr (B3LYP)/6-311G(d,p) level, revealed some peculiar structural factors governing the carbohydrate–matrix interaction.

Experimental

Chemicals and material

The *β*-carboline 9*H*-pyrido[3,4-*b*]indole (*nor*-harmane, nHo), 2,5-dihydroxybenzoic acid (GA) and the *E*-cinnamic acids (*E*-4-hydroxycinnamic acid [*trans*-coumaric acid; *E*-CuA], *E*-3-methoxy-4-hydroxycinnamic acid [*trans*-FA; *E*-FA] and *E*-3,5-dimethoxy-4-hydroxycinnamic acid [*trans*-SA; *E*-SA]) were purchased from Aldrich (USA). The sulfated neocarrabiose oligosaccharides [neocarratetraose 4^1,4^3-disulfate disodium salt (NCT); neocarrahexaose 4^1,4^3,4^5-trisulfate trisodium salt and neocarraoctaose 4^1,4^3,4^5,4^7-tetrasulfate tetrasodium salt) were purchased form Sigma-Aldrich (USA). The cyclomaltoheptaoses (*β*-cyclodextrin [b-CD], methyl-β-cyclodextrin [Mb-CD], heptakis(2,6-di-*O*-methyl)-*β*-cyclodextrin [DMb-CD], heptakis(2,3,6-tri-*O*-methyl)-*β*-cyclodextrin [TMb-CD] and 2-hydroxypropil-*β*-cyclodextrin [OHPb-CD]), glucose (Glu) and maltoses (maltose [M2], maltotriose [M3], maltotetraose [M4], maltopentaose [M5], maltohexaose [M6] and maltoheptaose [M7]) were obtained from Sigma Chemical, Tokyo, Japan. Fructans [fructose (F1), sucrose (F2), 1-kestose (F3), nystose (F4) and 1^F-fructofuranosylnystose (F5)] were obtained from Wako Pure Chemical Industries, Japan. The general structure of the carbohydrates studied is shown in Scheme S2. All the solvents (J. T. Baker HPLC grade) were used as purchased without further purification. Water of very low conductivity (Milli-Q grade) was used. *Z*-Cinnamic acids [*Z*-4-hydroxycinnamic acid (*Z*-coumaric acid, *Z*-CuA), *Z*-3-methoxy-4-hydroxycinnamic acid (*Z*-ferulic acid, *Z*-FA) and *Z*-3,5-dimethoxy-4-hydroxycinnamic acid (*Z*-sinapinic acid, *Z*-SA)] were synthesized as described elsewhere[16,17] and verified by m.p., ^{1}H-NMR and ^{13}C-NMR, UV–*vis* absorption spectroscopy and HRMS.[16]

Sample preparation

Matrix stock solutions were made by dissolving 2 mg of the selected compound in 1 mL of methanol/water (65 : 35. v/v). Analyte solutions were freshly prepared by dissolving the carbohydrates (1 mg) in water (1 mL). To prepare the analyte–matrix sample, the thin-film layer method (sandwich method)[26] was used. Typically 0.5 μL of the matrix solution was placed on the sample probe tip and air-dried at room temperature. Subsequently, 0.5 μL of the analyte solution was placed on the sample probe tip covering the matrix and partially dissolving it and air-dried. Then, two additional portions (0.5 μL) of matrix solution were deposited on the same sample probe tip, producing a partial dissolution of the previously deposited thin film. The matrix to analyte ratio was 3 : 1 (v/v), and the matrix and analyte solution loading sequence was (1) matrix, (2) analyte, (3) matrix and (4) matrix. Comparative experiments were also conducted preparing the analyte–matrix sample by the mixture method. The pre-prepared mixture was performed by mixing the matrix and analyte solutions in a 3 : 1 (v/v) ratio. Two portions (0.5 μL) of the mixture were successively loaded on the probe and air-dried at room temperature. Similar results were obtained with both sample preparation methods. The b-CD, M3 and F3 were chosen for the determination and comparison of the experimental limit of detection (LOD) achievable with GA, nHo, *Z*-SA and *E*-SA, in positive ion mode. Serial dilutions of an aqueous stock solution of the carbohydrate (1.2 mM) with water were carried out and analyzed. The lowest concentration tested was 1.2 μM. A 0.5 μL aliquot of the analyte solution was spotted on a dry layer prepared with 0.5 μL of matrix solution (GA, nHo, *Z*-SA or *E*-SA) following the general method for sample preparation described earlier. The monitoring ion was $[M + Na]^+$ ($[b\text{-}CD + Na]^+$, $[M3 + Na]^+$ and $[F3 + Na]^+$, respectively). Similar LOD experiments were conducted in negative ion mode using stock aqueous NCT solution (1.2 mM) successively diluted with water. The lowest concentration tested was 1.2 μM. The ion monitored was $[M - Na]^-$ ($[NCT - Na]^-$). LOD was defined as the pmol of analyte (b-CD, M3, F3 or NCT) transferred on the probe, which yielded a signal-to-noise ratio (S/N) that was S/N ≥ 4 (Table 1).

E-SA and *Z*-SA sample preparation on the probe for laser irradiation

A drop (0.5 uL) of SA (*E*-SA or *Z*-SA) solution in methanol/water (65 : 35, v/v) (4.77×10^{-9} M) was loaded on each spot of the probe (9.62 $mm^2 \times 32$). After laser irradiation of 16 spots (355 nm; automatic scan method, successive 1000 shots per spot ×20), the remaining solid was taken with methanol (1 mL) and was transferred to a 0.1-cm path length quartz cell (QTY 3, Type 21, Mat Q, Hellma). Besides, the solid deposited on the 16 spots not irradiated was taken with methanol (1 mL) and used as reference solution. The concentration of the initial solution and the number of total spot loaded and irradiated (×16) were adjusted in order to have enough amount (moles) of the remaining material on the probe to measure the corresponding

Table 1. Dynamic range and limit of detection of b-CD, M3 and F3 in the positive ion mode and of NCT in the negative ion mode using different matrices[a]

Matrix	b-CD[b] dynamic range LOD	M3[b] dynamic range LOD	F3[b] dynamic range LOD	NCT[c] dynamic range LOD
Z-SA	3.6–1200 3.6	9.6–1200 9.6	7.2–1200 7.2	4.8–1200 4.8
E-SA	?–1200[d]	?–1200[d]	?–1200[d]	ND[e]
GA	2.4–1200 2.4	4.8–1200 4.8	3.6–1200 3.6	3.6–1200 3.6
nHo	4.8–1200 4.8	6.0–1200 6.0	7.2–1200 7.2	48–1200 48

LOD, limit of detection.
[a]Indicated as pmol of carbohydrate deposited on the probe; S/N ≥ 4.
[b]Positive ion mode; β-cyclodextrin: b-CD; maltotreose: M3; 1-kestose: F3; monitoring ion $[M + Na]^+$.
[c]Negative ion mode; neocarratetraose $4^1,4^3$-disulfate disodium salt: NCT; monitoring ion $[M - Na]^-$.
[d]No linearity was observed; LOD could not determined.
[e]ND, no signal was detected.

UV-absorption spectrum. Spectra were also run after adding ethanolamine (61 μL; 0.166 M in methanol) to the stock methanol solution (standard solutions), to the reference solution and to the solution prepared with the remaining material obtained after laser irradiation experiments. *E*-SA and *Z*-SA show characteristic UV-absorption spectra in methanol/ethanolamine solution[27] as well as ^{1}H-NMR spectra.[16] Thus, ^{1}H-NMR spectroscopy was also used for monitoring these experiments.

MALDI-MS experiments

Spectra were recorded on a Bruker Ultraflex II TOF/TOF and controlled by the FLEXCONTROL 3.0 software (Bruker Daltonics, Bremen, Germany). Desorption/ionization was performed using a frequency tripled Nd: YAG laser emitting at 355 nm with a 100 Hz shot frequency. All mass spectra described were taken in the linear mode. Experiments were performed using firstly the full range setting for laser firing position in order to select the optimal position for data collection and secondly fixing the laser firing position in the sample sweet spots. The laser power was adjusted to obtain high S/N while ensuring minimal fragmentation of the parent ions, and each mass spectrum was generated by averaging 200 laser pulses per spot. Spectra were obtained and analyzed with the programs FLEXCONTROL and FLEXANALYSIS, respectively. MTP 384 target plate steel T F was used [part number: 209519; target frame (#74115); 384 circular spots, 3.5 mm diameter; S/N 03630].

UV-visible absorption spectroscopy

UV-visible absorption spectra of the matrix methanolic solutions were recorded on a Shimadzu UV-1203 spectrophotometer. Measurements were made in quartz cells of 1 and 0.1 cm optical path length (Hellma, Germany). Spectra were acquired from methanolic 10^{-5} to 10^{-2} M cinnamic acids solutions.

Molecular modeling

The ground state geometry of *Z*-cinnamic and *E*-cinnamic acids, GA and glucose (Glu) were fully optimized without imposing any symmetry constraints by *ab initio* and semiempirical methods (Scheme 2). For *ab initio* density functional theory calculations, we used the hybrid gradient-corrected exchange functional combined with the gradient-corrected correlation functional, commonly known as B3LYP, which has been shown to be quite reliable for geometries. For geometry optimization, the standardized 6-311G(d,p) basis set was used. We denote our B3LYP calculations by B3LYP/6-311G(d,p). For single point calculations, the standardized 6-311++G(d,p) basis set was used

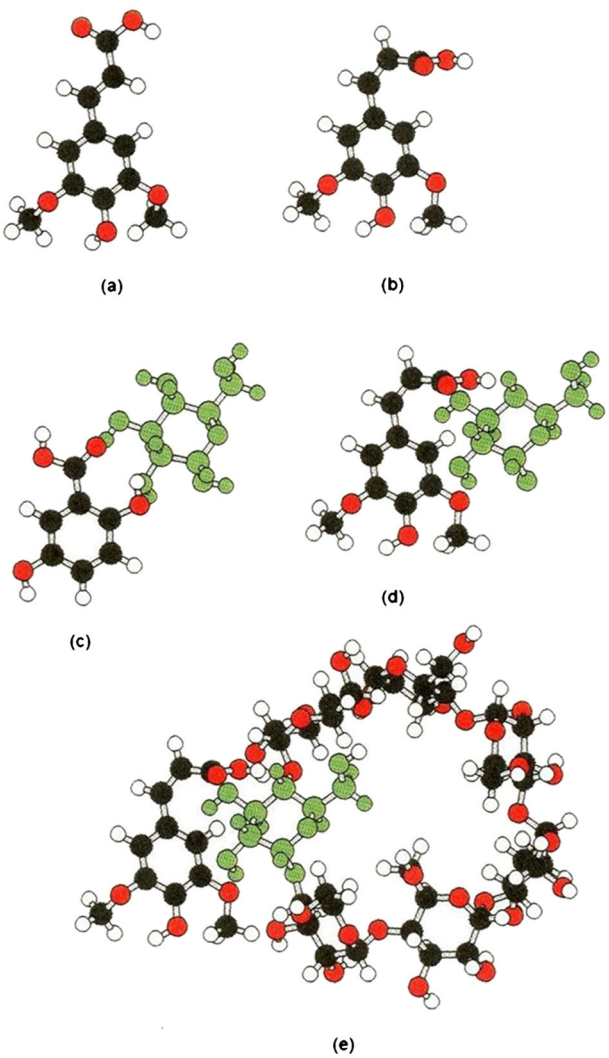

Scheme 2. Optimized geometries, (a) *E*-SA, (b) *Z*-SA and proposed analyte–matrix structures for (c) GA + glucose (GA + Glu), Glu in green, (d) *Z*-SA + glucose (*Z*-SA + Glu), Glu in green and (e) *Z*-SA + b-CD, maltose unity in the b-CD in green.

Journal of MASS SPECTROMETRY

at B3LYP theory level (B3LYP/6-311++G(d,p)/B3LYP/6-311G(d,p). All the *ab initio* calculations were carried out using Gaussian 98W program.[28]

The ground-state geometry of b-CD and dimeric structures shown in Scheme 2(c–e) were calculated by using the semiempirical parameterized PM3 method as implemented in the version of the HYPERCHEM 8.08 for Windows program[29] (Restricted Hartree–Fock formalism; total charge: 0; spin multiplicity: 1; convergence limit: 1e-008; iteration limit: 50; accelerate convergence: on; CI method: none; Polak-Ribiere algorithm; root mean square gradient: 0.006 kcal/(Å mol); in vacuo).

Results and discussion

The rationale of the original approach followed here was to synthesize various matrix candidates keeping in the aromatic ring (Ar) of the cinnamic acid core the nature and positions of the substituents (R1, R2 and R3) attached to the phenyl group (Ph) but modifying the geometry of the alkene moiety (Scheme 1). As a consequence in cinnamic acids, the stereochemistry of the molecule drastically changes too [i.e. *E*-SA and *Z*-SA, Scheme 2, structures (a) and (b)]. This property seems to play an important role in the analyte–matrix molecular interaction (refer to the succeeding texts).

Characteristics of the investigated matrices

Physical properties [m.p., UV-absorption spectra, ^{1}H-NMR, ^{13}C-NMR, EI-MS and HRMS (ESI-MS)] for the characterization of *E*-cinnamic and *Z*-cinnamic acids and *Z*-cinnamic acid synthesis have been described elsewhere.[16,17] Here is important to note that (1) in all cases, the m.p. of the *E*-isomer is higher than that of the *Z*-isomer, i.e. *E*-SA 185 °C and *Z*-SA 116–118 °C[16], and (2) the UV-absorption spectra in methanol solution for the *E*-isomer and *Z*-isomer are quite similar, i.e. λmax (nm) (log ε): *E*-SA 322 (4.14) and *Z*-SA 317 (4.01) (10^{-5}–10^{-4} M; Beer–Lambert conditions,[13,14]). UV absorption spectra were also acquired increasing matrix concentration, beyond the Beer–Lambert conditions.[13,14] The bands were getting wider and wider showing a bathochromic shift (red shift). At higher concentration (10^{-3}–10^{-2} M) and as an extrapolation in solid state, *E*-SA and *Z*-SA absorb efficiently at longer wavelengths including 355 nm (Fig. S1). For morphological inspection of the solid matrix deposited on the probe, the dried droplet method was used to prepare the sample. Fresh matrix solution was prepared in methanol/water as detailed in the Experimental Section. As a result, *E*-SA gave small crystals distributed at random, as aggregates, all over the sample surface (Fig. 1(a)), and *Z*-SA showed the aspect of a solid solution (glass) with few tinny heterogeneous round spots (Fig. 1(b)). When solid analyte–matrix sample was prepared on the probe with *E*-SA and *Z*-SA, the crystalline aspect of each sample was similar to that of the matrix alone (Fig. 1). Digital images were registered on the Bruker Ultraflex II TOF/TOF.

MALDI mass spectrometry analysis

Matrices

Laser desorption/ionization experiments were conducted with the 355 nm laser on the Bruker Ultraflex II TOF/TOF in positive and negative ion modes. Experiments were run in exactly the same conditions (solution concentration, solvent, volume loaded on the probe, NaCl added in doped experiments, experimental parameter etc.). In both ion modes, the laser energy applied (laser power) was slightly above the ionization threshold and similar to that used in experiments conducted for carbohydrate analysis.

As shown in Fig. 2(a) and (b), positive ion mode *Z*-SA always showed more abundant peaks than *E*-SA. Experiments without adding NaCl: the spectrum of *E*-SA showed the protonated intact molecular ion peak at m/z 225.42 $[M+H]^+$ and the predominant signal at m/z 207.37 (base peak) assigned to the species $[M-OH]^+$ as well as peaks at higher m/z corresponding to $[M+Na]^+$ (247.60) and at m/z 285.56 (not assigned) (Fig. 2(b)). *Z*-SA (Fig. 2(a)) showed signals at m/z 207.13 $[M-OH]^+$, 225.40 $[M+H]^+$ (small peak), 247.43 $[M+Na]^+$, 263.61 $[M+K]^+$ and signals not assigned at m/z 269.43, 285.53 (base peak) and 301.77. Experiments adding NaCl (0.01–1M): when samples were doped with NaCl, additional signals at m/z 22.95 $[Na]^+$, 38.89 $[K]^+$ and 269.06 were observed in the LDI spectrum of *E*-SA (base peak at m/z 207.33) (Fig. 2(d)), while for *Z*-SA, additional signal at 22.62 $[Na]^+$ and 38.40 $[K]^+$ together with cluster signals at m/z 308.89, 335,28 and 368,45 were observed (base peak at 284.42) (Fig. 2(c)). In negative ion mode, the spectra of *E*-SA and *Z*-SA were quite simple and similar. The $[M-H]^-$ species and the deprotonated dimeric cluster at m/z 223.17 and 447.44 for the former and at m/z 223.10 and 447.36 for the latter were observed (Fig. 2(e) and 2(f)). In this mode, NaCl addition did not affect the spectra. Similar LDI results were obtained for the *E*-form/*Z*-form of the other cinnamic acids studied (FA and CuA; results not shown).

Neutral carbohydrates

To begin with our comparative study of the application of *E*-SA and *Z*-SA as MALDI matrices for analysis of carbohydrates, their performances as matrices for commercially available fructans, maltoses, cyclodextrines and sulfated sugars were investigated (analytes are

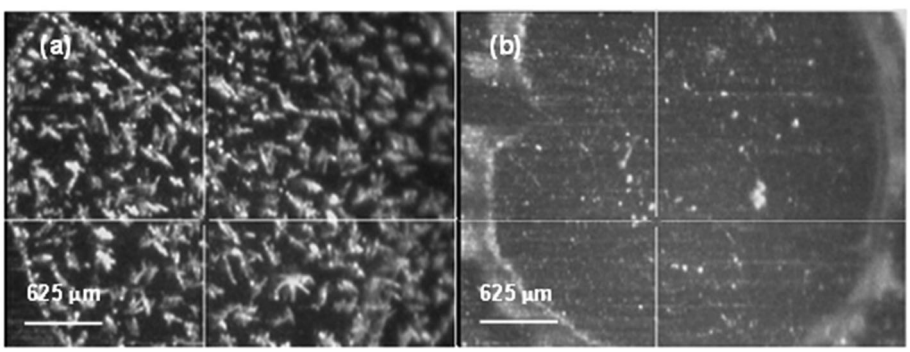

Figure 1. Morphology (a) *E*-SA and (b) *Z*-SA. Circular spot surface, 9.62 mm^2. Digital images from Bruker Ultraflex II TOF/TOF.

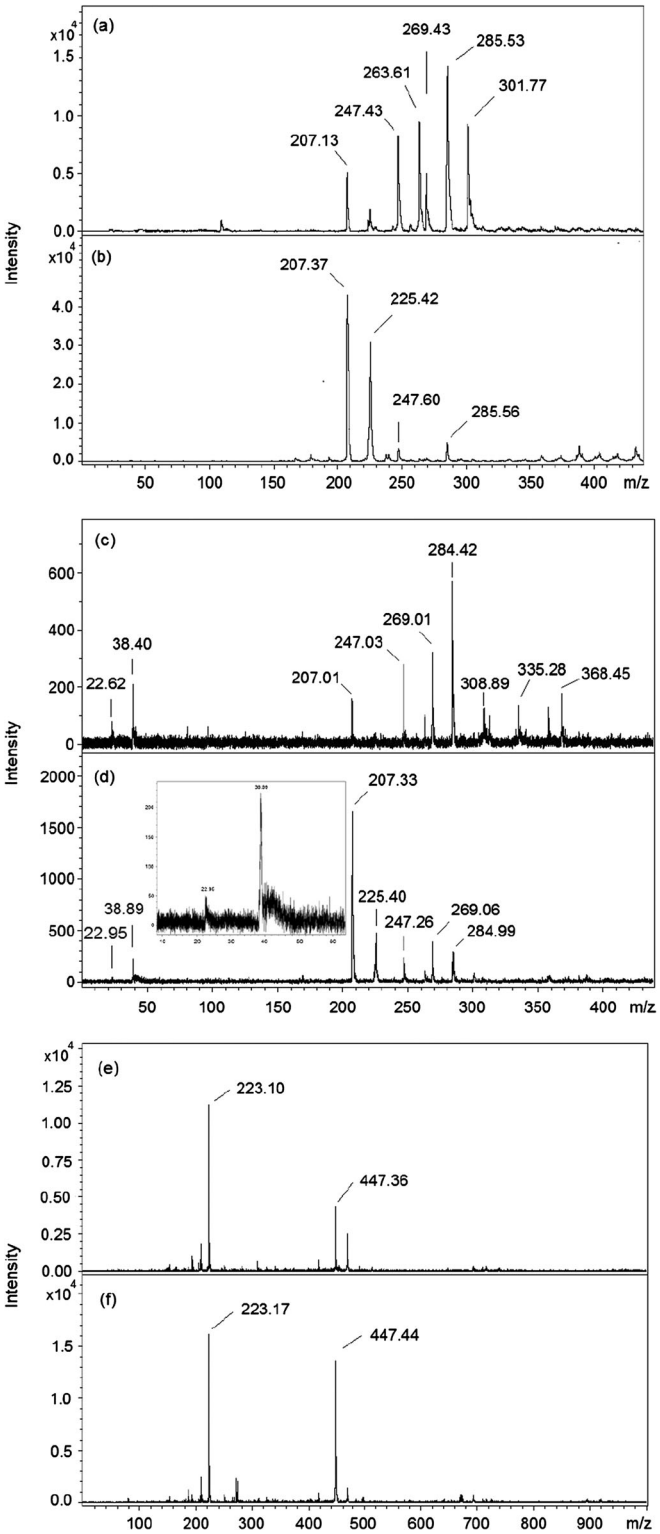

Figure 2. Laser desorption/ionization mass spectra. Positive ion mode: (a) *Z*-SA, (b) *E*-SA, (c) *Z*-SA + NaCl and (d) *E*-SA + NaCl. Negative ion mode: (c) *Z*-SA and (d) *E*-SA. Laser λem: 355 nm, power 60%. SA, m.w. 224.21.

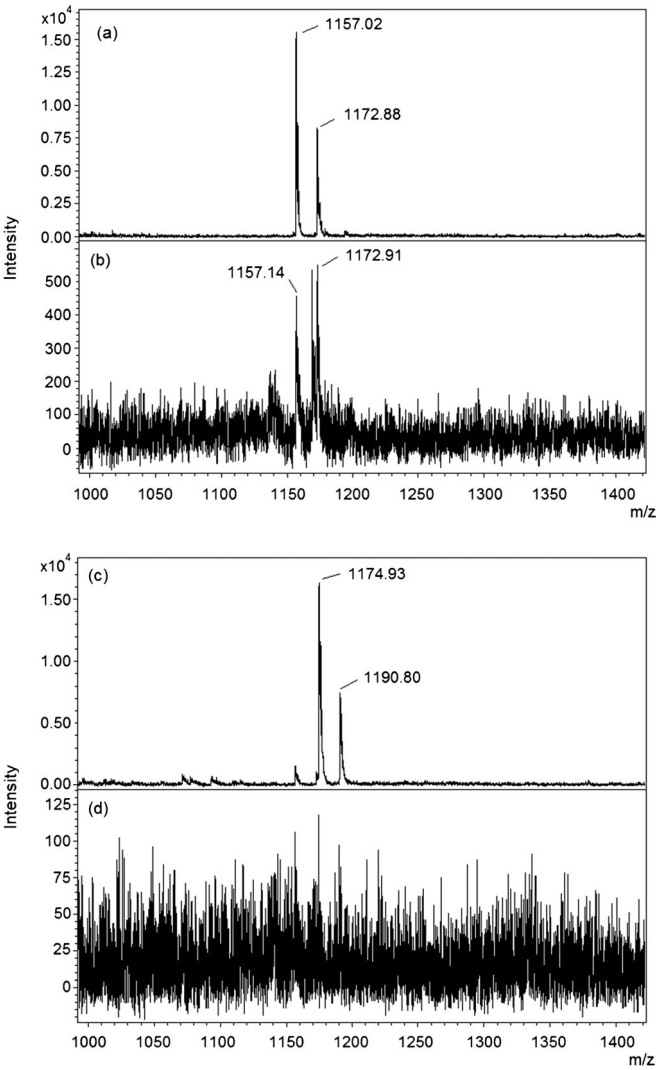

Figure 3. MALDI mass spectra of neutral carbohydrates: (a) b-CD, matrix: *Z*-SA; (b) b-CD, matrix: *E*-SA; (c) M7, matrix: *Z*-SA and (d) M7, matrix: *E*-SA. Positive ion mode. Monitoring ions $[M+Na]^+$ and $[M+K]^+$. No NaCl added.

listed in the Experimental Section; general molecular structure of the compounds studied are included in Scheme S2).

As an example, in Fig. 3, the spectra obtained in positive ion mode by deposition of solution of β–cyclodextrin (b-CD) (Fig. 3 (a) and (b)) and of maltoheptaose (M7) (Fig. 3(c) and (d)) on air-dried layers of the examined matrix (sandwich method) are shown (monitored ions $[M+Na]^+$ and $[M+K]^+$. We used b-CD and M7 aqueous solutions without any salt added (not salt doped). Experiments were conducted in positive and negative ionization modes. Best results were obtained in the former. As can be seen, the efficiency of the desorption/ionization of each carbohydrate as mono-sodiated species ($[M+Na]^+$) and mono-potassiated species ($[M+K]^+$) as well as the clusters observed depend on the SA isomer used as matrix, i.e. *Z*-SA (Fig. 3 (a) and (c)) showed to be a better matrix than *E*-SA (Fig. 3(b) and (d)). When the other neutral maltoses, fructanes and substituted β-cyclodextrines were checked always, *Z*-SA performed better as matrix (refer to the examples for F4, M2, Mb-CD, HOPb-CD and F2 in Figs S2–S6). In all cases, abundant sweet spots were easy to find, homogenously distributed all over the sample surface for *Z*-SA, whereas they were a few and difficult to find or just that we could not find at all for *E*-SA. Similar results were obtained with the other cinnamics studied (i.e. Figs S7 and S8; analyte, M7 with *Z*-FA, *E*-FA, *Z*-CuA and *E*-CuA as matrices; positive ion mode).

Journal of MASS SPECTROMETRY

We have examined the tolerance of the matrices *Z*-SA and *E*-SA towards the extra amount of NaCl in the samples. We found that both compounds show similar behavior as matrix, in the positive ion mode, with and without extra NaCl added, i.e. almost the same spectra as those shown in Fig. 3(a) and (b) were obtained for b-CD with *Z*-SA and with *E*-SA, adding NaCl (up to 0.1 M solution). In all cases, the addition of NaCl diminished the relative intensity of the signal $[M + K]^+$ but did not increase the absolute intensity of the signal $[M + Na]^+$. As a conclusion, even doping the sample with NaCl, *Z*-SA performed better than matrix *E*-SA.

Sulfated carbohydrates

Sulfated oligosaccharide MALDI-MS analyses were conducted in both ion modes. Best results were obtained in negative ion mode. The application of the *E*-SA, *Z*-SA, GA and nHo(9*H*-pyrido[3,4-*b*] indole, nHo) for sulfated oligosaccharides demonstrated that *Z*-SA showed good performance in terms of sensitivity and suppression of ISD of the sulfate groups as GA did and both behaved better than nHo in negative ion mode. On the contrary, the performance of *E*-SA was the worst. When *E*-SA was used, intact molecular ions as $[M - Na]^-$ and the corresponding main fragments were not detected or just as very minor signals. The fragmentation in negative ion mode mainly occurred by the dissociation of the sulfate groups according to a loss of 102 Da from the $[M - Na]^-$ to yield $[M - Na - nSO_3Na + nH]^-$ (i.e. Frag. $1 = [M - Na - SO_3Na + H]^-$, Frag. $2 = [M - Na - 2SO_3Na + 2H]^-$, etc.).[24,25] As an example, in Fig. 4, the spectra obtained in negative ion mode for neocarratetraose $4^1,4^3$-disulfate disodium salt (m.w. 834.62; general molecular structure for sulfated carbohydrates is included in Scheme S2) with three different matrices are displayed. It can be observed the significant suppression of dissociation of the sulfate groups using *Z*-SA (Fig. 4(a)) and GA (Fig. 4(b)) and the importance of ISD when nHo was the matrix (hot matrix) (Fig. 4(c); ions observed: $[M - Na]^-$ at m/z 811.30 and $[M - Na - SO_3Na + H]^-$, Frag. 1, at m/z 709.61). Analyte signals were not detected when *E*-SA was the matrix (results not shown). Additional figures comparing the spectra obtained for neocarrahexaose $4^1,4^3,4^5$-trisulfate trisodium salt (m.w. 1242.95) using *Z*-SA, GA and nHo as matrix (Fig. 4(d–f)) and neocarraoctaose $4^1,4^3,4^5,4^7$-tetrasulfate tetrasodium salt (m.w. 1651.26) (Fig. 4(g–i)) using *Z*-SA, *E*-SA and nHo as matrix are displayed.

As a conclusion of this section, *Z*-SA behaved quite similarly to GA in the analysis of sulfated sugars in negative ion mode, and we can call it 'cold' matrix too (suppression of ISD). The additional advantage was that all over the sample prepared with *Z*-SA, sweet spots were homogeneously distributed and were easily to find.

Dynamic range, linearity and limit of detection determination

Dynamic range, linearity and LOD studies for neutral sugars were conducted in positive ion mode. Figure 5(a) shows the comparison between the results obtained for 1-kestose (F3) deposited on the examined matrices, *Z*-SA and *E*-SA and on a crystalline organic matrix currently used for carbohydrate analysis, GA. The intensity of the mono-sodiated ion $[M + Na]^+$ in the positive ion mode was monitored. The dynamic ranges in which carbohydrate signal was detected with good S/N ratios (S/N ≥ 4) are listed in Table 1. Results obtained using nHo as matrix are also included in this table. *Z*-SA showed satisfactory LOD and dynamic range, although the intensity of the signals was lower than those obtained with GA in all the range studied (Fig. 5(a)). As shown in Fig. 5(b), *E*-SA was not efficient at all, as matrix and in the range

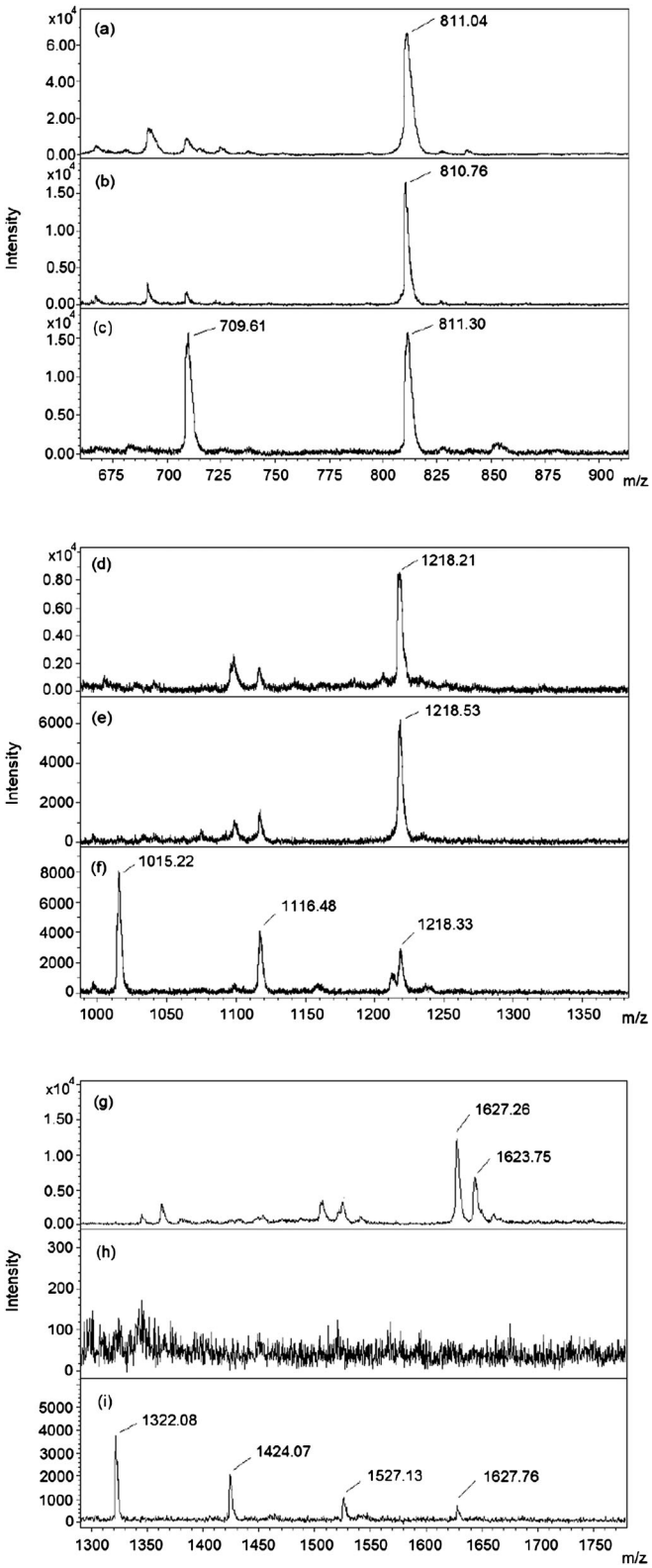

Figure 4. MALDI mass spectra of sulfated carbohydrates: NCT (m.w. 834.62), matrix: (a) *Z*-SA, (b) GA and (c) nHo. NCH (m.w. 1242.95), matrix: (d) Z-SA, (e) GA and (f) nHo. NCO (m.w. 1651.26), matrix: (g) *Z*-SA, (h) *E*-SA and (i) nHo. Negative ion mode. Monitoring ion $[M - Na]^-$.

of concentrations studied (Table 1, 1.2 μM–1.2 mM), $[M + Na]^+$ signal was very low or not detected. For b-CD and maltotriose (M3), we conducted experiments in positive ion mode, and

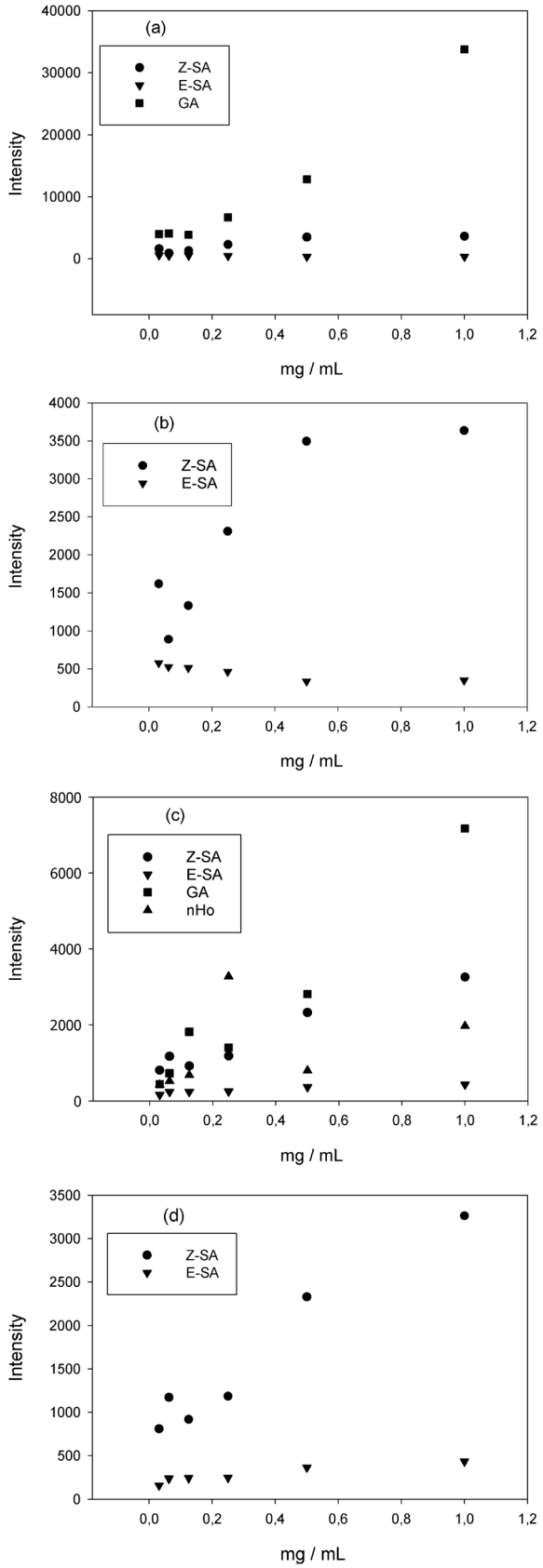

Figure 5. Dynamic range and intensity *versus* concentration ratio. Positive ion mode: 1-kestose (F3), matrix: (a) *Z*-SA, *E*-SA and GA; (b) Z-SA and *E*-SA. Monitoring ion $[M + Na]^+$. Negative ion mode: neocarratetraose 4,4′-disulfate disodium (NCT), matrix: (c) Z-SA, *E*-SA, GA and nHo; (d) Z-SA and *E*-SA. Monitoring ion $[M - Na]^-$.

similar conclusions were reached (Table 1, Figs S9 and S10). As a summary in Fig. 6, it shows the capability of *Z*-SA and *E*-SA to reproduce b-CD signals compared with those of GA and nHo when data were collected in the same position of a spot (each point is the average intensity value of ten laser shots on the fixed position on the sample) and data collected in different positions of a spot (each point is the average intensity value of 100 laser shots on different positions on the sample).

In the negative ion mode dynamic range, linearity and LOD studies were also performed using nHo and GA as reference matrices. As it was mentioned for both *E*-SA and *Z*-SA as matrices, molecular ions of fructans, maltoses and b-CD as $[M - H]^-$ were poorly detected or not detected at all. On the contrary, sulfated sugars were better detected (high ionization efficiency, good reproducibility and good S/N ratio) in negative ion mode as the species $[M - Na]^-$. Thus, for sulfated sugars, experiments were conducted in this ionization mode, and the intensity of the ion $[M - Na]^-$ was monitored. As shown in Fig. 5(c), linearity with *Z*-SA for neocarratetraose 4,4′-disulfate disodium was better than with nHo. This result was expected because the important ISD

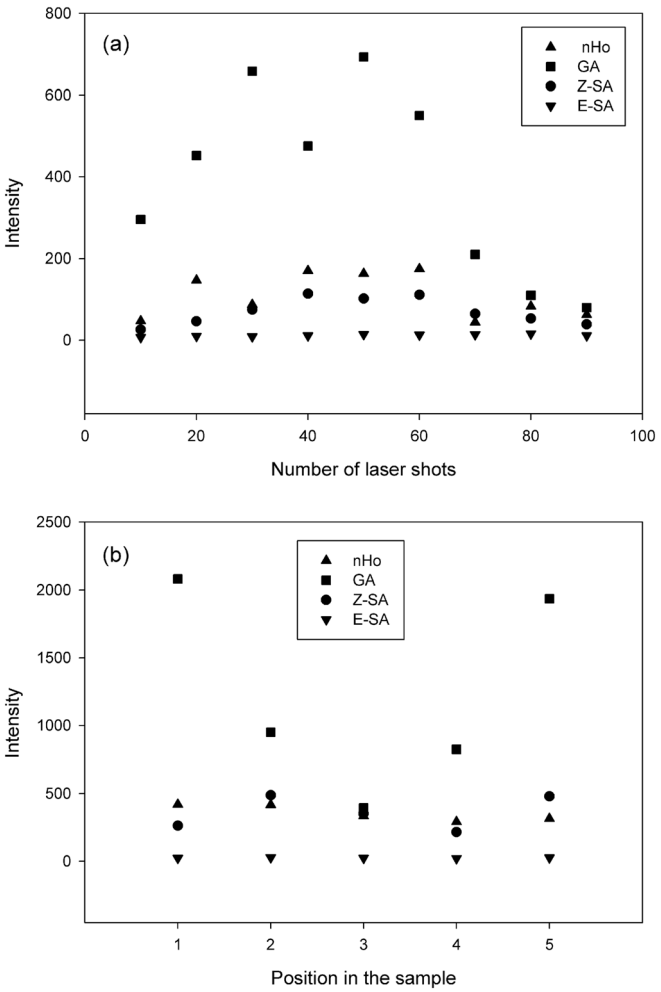

Figure 6. Capability of *Z*-SA to reproduce b-CD signals compared with that of *E*-SA, GA and nHo. Panel (a): all data were collected in the same position of a spot; each point represents the average intensity value of ten laser shots on the fixed position on the plate. Panel (b): data were collected in different positions of a spot; each point represents the average intensity value of 100 laser shots on a position on the plate. Signal intensity of $[b\text{-}CD + Na]^+$ was monitored. Positive ion mode.

induced by nHo (Fig. 4(c)). The results of examining the ratios of signal intensities to the concentrations of standard sugar deposited on the matrix showed a remarkable concentration-sensitivity, especially in the cases of GA and *Z*-SA. On the contrary, *E*-SA did not exhibit linearity, and the intensity of the signal was practically independent of the carbohydrate concentration in the tested solution (Fig. 5(d)). Similar results for *E*-SA are shown in Fig. 5(a–b), S9 and S10. Furthermore, in some examples with increasing amount of carbohydrate deposited on *E*-SA, the desorption/ionization efficiency of the carbohydrate decreased (the absolute intensity of the signal decreases instead of increases; Fig. S10, increasing the M3 concentration in the aqueous solution, i. e. from 0.3 to 1.2 mg/mL). The examined matrices (*Z*-SA, GA and nHo), except for *E*-SA, showed different linearity between the concentration of each neutral carbohydrate (maltotriose, 1-kestose and b-CD) and its $[M + Na]^+$ signal intensity in the positive ion mode (Fig. 5(a-b), S9, and S10) and its $[M - Na]^-$ signal intensity in the negative ion mode, in the case of sulfated carbohydrates (i.e. NCT, Fig. 5(c–d)).

As a summary, Table 1 shows the dynamic range and LOD obtained in both ion modes. Samples were not doped (no salt added) because higher intensity signals were observed in this experimental conditions. Doping by NaCl did not significantly improve the LOD in any ion mode (results not shown). *Z*-SA, GA and nHo showed comparably satisfactory LODs and dynamic ranges for the neutral carbohydrates studied, and they were superior to *E*-SA. In the negative ion mode, *Z*-SA and GA performed better than nHo, and *Z*-SA was the worst. The superiority of the *Z*-SA as matrix in both ion modes and the similarity in the latter mode to GA (cold matrix) probably originate from *Z*-SA capability to participate in a special analyte–matrix interaction at molecular level (Scheme 2(c–e)).

Inspection of the matrix behavior under successive laser shots in the same probe position

MALDI mass spectra. The *E*/*Z* photoisomerization (Scheme S1) has been described in different media.[7–17] In order to inspect this possibility for *E*-cinnamic and *Z*-cinnamic acids in the solid analyte–matrix sample during MALDI mass spectrometry analysis, different experiments were conducted. The b-CD was used as analyte. Solid samples were prepared according to the method described in the Experimental Section as b-CD + *E*-SA. The analysis was conducted in positive ion mode, shotting at a fixed position of the sample. The intensity of the signal $[b\text{-}CD + Na]^+$ was monitored. The low intensity and poor resolution signal detected with *E*-SA did not improve after successive shots (100, 200, 300, 400, 500) at the same sample position (Fig. S11(a)). When similar experiments were conducted with *Z*-SA as matrix (Fig. S11(b)), the higher intensity and better S/N ratio of the signals compared with those obtained with *E*-SA (Fig. S11(a)) were kept after successive shots although the absolute intensity of the signals diminished because of sample consumption (Fig. S11(b)). Similar experiments were conducted, as comparative experiments, using nHo and GA as matrices (Fig. S11(c) and (d)).

On the contrary, the behavior of *E*-SA as matrix drastically improved when mixtures of *E*-SA and *Z*-SA were used as matrix. The solid sample was prepared as analyte + *E*-SA + *Z*-SA, getting better results when the mixture was enriched in the *Z* isomer (i.e. *E*-SA and *E*-SA : *Z*-SA 9 : 1; Fig. S12(c) and (b)). The trend of S/N ratio for the $[b\text{-}CD + Na]^+$ signals obtained according to the matrix used was *Z*-SA >> *E*-SA : *Z*-SA 9 : 1 > *E*-SA. Results obtained by using M7 as analyte were similar (results not shown).

As a conclusion, the *E*-photoisomerization to *Z*-photoisomerization would not be an important process in the solid state during the MALDI process.

Solid remaining on the probe. The photochemical behavior of *E*-SA and *Z*-SA in solid state was inspected in several experiments. The *E*-SA solid deposited on the MALDI probe was laser shotted all over the spots' surface (refer to the details in the Experimental Section). The solid remaining was washed from the surface with methanol, and the UV-absorption spectrum was recorded. The maximum of absorbance was located at a similar value than that of the *E*-SA (fresh solution) although the absorbance intensity diminished. After adding water to the solution, the expected shift to lower wavelength, characteristic of *Z*-SA, was not observed. After adding ethanolamine to the solution, the expected shift to lower wavelength, characteristic of *Z*-SA, was not observed either[27] (Fig. S13(a) and (b)). Similar experiment conducted with *Z*-SA showed a higher ablation of the matrix, and the remaining solid in methanol solution did not show the presence of *E*-SA. On the contrary, the maximum showed the typical shift of the *Z*-SA (Fig. S13(a) and (b)). In parallel experiments, the remaining solid material in $(CD_3)_2SO$ solution by ^{1}H-NMR analysis showed the presence of only *E*-SA in the former and *Z*-SA in the latter (Fig. S14(a) and (b)). In these experiments, the photo dimer products were not detected (Scheme S1).

Stereochemistry – molecular modeling

By using molecular modeling, special attention was paid on the stereochemistry of *Z*-cinnamic and *E*-cinnamic acids. The optimized geometry for *E*-cinnamic acids showed a preferential almost flat and rigid molecule as shown in Scheme 2(a) for *E*-SA. On the contrary, *Z*-cinnamic acids showed that the carboxylic group rotates and approaches the polar substituents located at C-3 and C-4 of the aryl group in a synclinal overlapping fashion to create a cavity limited by the polar substituents and the carboxylic group (i.e. *E*-SA in Scheme 2(b)). The cavity provides the required distance among the functional groups located at the entrance to allow the inclusion of a monosaccharide molecule and the generation of stabilizing intermolecular interactions such as hydrogen bonds with it. As shown in Scheme 2 (d) (*Z*-SA + Glu), this approach and interactions can easily occur with a small monosaccharide such as hexose and/or pentose, i. e. glucose (Glu) and with any of the monosaccharide units included in an oligosaccharide such as β–cyclodextrin (b-CD) and higher m.w. oligosaccharides and polysaccharides (Scheme 2(e), monosaccharide unit in green). This would be the first level of control of matrix-analyte molecular interaction in the solid sample when *Z*-SA is used as matrix. There would be a selective interaction of *Z*-SA with carbohydrate basic structure; thanks to its peculiar stereochemistry. This special interaction at crystal molecular level is not possible with *E*-SA because of its planar semirigid structure. A second level of control and differentiation of the process could be imparted through the higher efficiency of desorption (ablation) showed by Z-SA and its lower m.p. Inspection by molecular modeling of the GA-glucosa interaction at molecular level showed the presence of a similar polar cavity defined by the –COOH group and the OH group located at C-2 in the aromatic ring (Scheme 2(c), glucose in green) where the monosaccharide can be located forming H bonds with both functional groups.

*Electronic excited states and E-Z-*photoisomerization

The lifetime of the singlet state is recognized as a critical parameter in all MALDI model discussions. The values for the singlet lifetimes of *E*-cinnamic and *Z*-cinnamic MALDI matrices measured in this work, in solution (results not shown), are as short as the values previously reported by Ehring and Sundqvist,[30,31] Alllwood and Dyer[32] and Ludemann *et al.*[33] for *E*-isomers. In the last publication,[33] the authors concluded that the short singlet lifetimes reported imply that the majority of singlet excited states would not survive the plume expansion and would react at near solid-state densities. Taking into account the possibility of the *E*-photoisomerization to *Z*-photoisomerization of the singlet excited state, if it took place in the plume, the *Z*-species formed did not have any influence on the ionization of the carbohydrates, because as we demonstrated, ionization efficiencies were quite different when *Z*-SA and *E*-SA were used independently as MALDI matrices. Furthermore, if *E*-photoisomerization to *Z*-photoisomerization took place earlier at near solid-state densities, *Z*-species formed did not have any influence on the ionization of the carbohydrates, because as we demonstrated clearly ionization efficiencies were quite different when *Z*-SA and *E*-SA were independently used.

According to our results, only the preexisting *Z*-SA in the ground state of the compound used as MALDI matrix is active to induce the efficient ionization of carbohydrates.

Conclusions

Results obtained allow to conclude that (1) *Z*-SA is a very good matrix for neutral/sulfated carbohydrate analysis on the contrary to that of *E*-SA, (2) Z-SA is a new cold matrix for sulfated carbohydrate analysis because suppression of ISD of sulfated sugars was observed, and (3) *E*-photoisomerization/*Z*-photoisomerization does not play a key role during the MALDI event in the carbohydrate analysis.

Molecular modeling as an additional tool showed that as a consequence of the geometry change in the alkene rigid bond of the cinnamic moiety, the stereochemistry of the matrix molecule changes dramatically and, at molecular level, the analye–matrix interaction too.

Although the performances of *Z*-FA and *Z*-CuA as matrices were not as outstanding as that shown by *Z*-SA in carbohydrate analysis, in all cases, the *Z*-isomer was better than the corresponding *E*-isomer (i.e. *Z*-FA better than *E*-FA, *Z*-CuA better than *E*-CuA; Figs S7 and S8). The number of substituents in the aromatic group seems to play an important role because the trend shown by the performance of the *Z*-isomers was *Z*-SA > *Z*-FA >> *Z*-CuA, not working cinnamic acid as matrix at all (results not shown). In connection with these results, molecular modeling showed that number and location of substituents in the aromatic group are quite critical because they control the number of simultaneous hydrogen bonds that can be formed by the carbohydrate molecule and the matrix molecule (1/1, molecule/molecule). Higher number of hydrogen bonds between the analyte and the matrix molecules might help the inclusion of the analyte in the matrix crystal structure, increasing the homogeneity of the distribution of analyte in the solid matrix and, as consequence, the number and homogeneous distribution of the sweet spots too.

The investigation of the performance of *Z*-SA and *E*-SA as MALDI matrices for carbohydrate MALDI mass spectrometry analysis provides important insights into the intrinsic MALDI process when cinnamic acids are used as matrices. The quite different performance of the cinnamic geometric isomers as matrices is described for the first time and could be used to investigate new aspects of the so dark and still quite unknown MALDI process. Meanwhile, studies of the possible application of *Z*-SA, *Z*-FA and *Z*-CuA as matrices for polypeptide and protein analysis are in progress in our laboratory.

Acknowledgements

The authors would like to thank the National Research Council of Argentina (CONICET; PIP 0400) and the University of Buenos Aires (UBA X088 and X01/J080) for the financial support. R. E. B. and M. L. S. are Research Members of CONICET (Argentina). The Ultraflex II (Bruker) TOF/TOF mass spectrometer was supported by a grant from Agencia Nacional de Promocion Cientifica y Tecnologica (ANPCYT), PME 125.

References

[1] R. C. Beavis, B. T. Chait. Cinnamic acid derivatives as matrices for ultraviolet laser desorption mass spectrometry of proteins. *Rapid Commun. Mass Spectrom.* **1989**, *3*, 432.
[2] R. C. Beavis, T. Chaudhary, B. T. Chait. α-Cyano-4-hydroxycinnamic acid as a matrix for matrix-assisted laser desorption mass spectrometry. *Org. Mass Spectrom.* **1992**, *27*, 156.
[3] K. Schneider, B. T. Chait. Matrix-assisted laser desorption mass spectrometry of homopolymer oligodeoxyribonucleotides. Influence of base composition on the mass spectrometric response. *IRapid Commun. Mass Spectrom.* **1993**, *28*, 1353.
[4] T. W. Jaskolla, W. D. Lehmann, M. Karas. 4-Chloro-α-cyanocinnamic acid is an advanced, rationally designed MALDI matrix. *Proc. Natl. Acad. Sci. U. S. A.* **2008**, *105*, 12200.
[5] T. Porta, C. Grivet, R. Knochenmuss, E. Varesioa, G. Hopfgartner. Alternative CHCA-based matrices for the analysis of low molecular weight compounds by UV-MALDI-tandem mass spectrometry. *J. Mass Spectrom.* **2011**, *46*, 144.
[6] B. B. Buchanan, W. Gruissem, R. L. Jones. Biochemistry & molecular biology of plants. American Society of Plant Physiologist, Rockville. **2000** Chapter 24, pp.1286.
[7] M. L. Salum, R. Erra-Balsells. High purity *cis*-cinnamic acid preparation for studying physiological role of *trans*-cinnamic and *cis*-cinnamic acids in higher plants (review). *Environ. Control in Biol.* **2013**, *51*, 1.
[8] T. Mori, Y. Inoue, in C=C Photoinduced Isomerization Reactions, A. G. Griesbeck and J. Mattay (Eds). Synthetic Organic Photochemistry, Marcel Dekker: New York, **2005**, 417.
[9] T. Arai. Organic molecular photochemistry. in Photochemical *cis*-Trans Isomerization in the Triplet State Vol 3, Molecular and Supramolecular Photochemistry, V. Ramamurthy and K. S. Schanze (Eds), CRC press: Boca Raton, Florida, USA, **1999**, 131.
[10] V. J. Rao. Organic molecular photochemistry. in Photochemical *cis*-Trans Isomerization from the Singlet State Vol 3. Molecular and Supramolecular Photochemistry, V. Ramamurthy, K. S. Schanze (Eds). CRC press: Boca Raton, Florida, USA, **1999**, 169.
[11] R. C. Nieuwendaal, M. Bertmer, S. E. Hayes. An unexpected phase transition during the [2+2] photocycloaddition reaction of cinnamic acid to truxillic acid: changes in polymorphism monitored by solid-state NMR. *J. Phys. Chem. B* **2008**, *112*, 12920.
[12] B. L. Feringa, R. A. van Delden, N. Koumura, E. M. Geertsema. Chiroptical molecular switches. *Chem. Rev.* **2000**, *100*, 1789.
[13] M. Klessinger, J. Michl. Excited States and Photochemistry of Organic Molecules, VCH Publishers, Inc.: New York, **1995**, 362.
[14] N. J. Turro, V. Ramamurthy, J. C. Scaiano. Principles of Molecular Photochemistry: An Introduction. University Science Books: Sausalito, **2009**, 319.
[15] A. Parthasarathy, S. R. Samanta, V. Ramamurthy. Photodimerization of hydrophobic guests within a water-soluble nanocapsule. *Res. Chem. Interm.* **2013**, *39*, 73.
[16] M. L. Salum, C. J. Robles, R. Erra-Balsells. Photoisomerization of ionic liquids ammonium cinnamates: one-pot synthesis-isolation of *Z*-cinnamic acids. *Org. Lett.* **2010**, *12*, 4808.

[17] M. L. Salum, R. Erra-Balsells. One-pot synthesis of *Z*-cinnamic acids. Argentine Patent, CONICET #20090105020, **2009**.
[18] Y. Gholipour, H. Nonami, R. Erra-Balsells. *In situ* analysis of plant tissue underivatized carbohydrates and on-probe enzymatic degraded starch by matrix-assisted laser desorption/ionization time-of-flight mass spectrometry by using carbon nanotubes as matrix. *Anal. Biochem.*, **2008**, *383*, 159.
[19] Y. Gholipour, S. L. Giudicessi, H. Nonami, R. Erra-Balsells. Diamond, titanium dioxide, strontium titanium oxide, and barium strontium titanium oxide nanoparticles for direct matrix assisted laser desorption/ionization mass spectrometry analysis of soluble carbohydrates in plant tissues. *Anal. Chem.*, **2010**, *82*, 5518.
[20] M. D. Mohr, O. K. Börnsen, H. M. Widmer. Matrix-assisted laser desorption/ionization mass spectrometry: improved matrix for oligosaccharides. *R. Commun. Mass Spectrom.* **1995**, *9*, 809.
[21] Y. Dai, R. M. Whittal, C. A. Bridges, Y. Isogai, O. Hindsgaul, L. Li. Matrix-assisted laser desorption ionization mass spectrometry for the analysis of monosulfated oligosaccharides. *Carbohydr. Res.* **1997**, *304*, 1.
[22] D. J. Harvey. Matrix-assisted laser desorption/ionization mass spectrometry of carbohydrates. *Mass Spectrom. Rev.* **1999**, *18*, 349.
[23] D. J. Harvey. Analysis of carbohydrates and glycoconjugates by matrix-assisted laser desorption/ionization mass spectrometry: an update covering the period 2007–2008. *Mass Spectrom. Rev.* **2012**, *31*, 183.
[24] Y. Fukuyama, S. Nakaya, Y. Yamazaki, K. Tanaka. Ionic liquid matrixes optimized for MALDI-MS of sulfated/sialylated/neutral oligosaccharides and glycopeptides. *Anal. Chem.* **2008**, *80*, 2171.
[25] Y. Fukuyama, M. Ciancia, R. Erra-Balsells, M. C. Matulewicz, H. Nonami, A. S. Cerezo. Matrix-assisted ultraviolet laser desorption ionization time-of-flight mass spectrometry of sulfated carrageenan oligosaccharides. *Carbohydr. Res.* **2002**, *337*, 1553.
[26] L. Li, R. E. Golding, R. M. Whittal. Analysis of single mammalian cell lysates by mass spectrometry. *J. Am. Chem. Soc.* **1996**, *118*, 11662.
[27] M. L. Salum, R. Erra-Balsells. Effect of water and aliphatic amines on the UV-absorption spectra of *E*- and *Z*-cinnamic acids in methanol solution (paper is under preparation).
[28] Gaussian 98W, Revision A.3., Gaussian 98, Revision A.3, M. J. Frisch, G. W. Trucks, H. B. Schlegel, G. E. Scuseria, M. A. Robb, J. R. Cheeseman, V. G. Zakrzewski, J. A. Montgomery, Jr., R. E. Stratmann, J. C. Burant, S. Dapprich, J. M. Millam, A. D. Daniels, K. N. Kudin, M. C. Strain, O. Farkas, J. Tomasi, V. Barone, M. Cossi, R. Cammi, B. Mennucci, C. Pomelli, C. Adamo, S. Clifford, J. Ochterski, G. A. Petersson, P. Y. Ayala, Q. Cui, K. Morokuma, D. K. Malick, A. D. Rabuck, K. Raghavachari, J. B. Foresman, J. Cioslowski, J. V. Ortiz, B. B. Stefanov, G. Liu, A. Liashenko, P. Piskorz, I. Komaromi, R. Gomperts, R. L. Martin, D. J. Fox, T. Keith, M. A. Al-Laham, C. Y. Peng, A. Nanayakkara, C. Gonzalez, M. Challacombe, P. M. Gill, B. Johnson, W. Chen, M. W. Wong, J. L. Andres, C. Gonzalez, M. Head-Gordon, E. S. Replogle, J. A. Pople, Gaussian, Inc., Pittsburgh PA, **1998**.
[29] HyperChem 8.08 for Windows, HyperCube Inc.: Ontario, **2010**.
[30] H. Ehring, B. U. R. Sundqvist. Studies of the MALDI process by luminescence spectroscopy. *J. Mass Spectrom.* **1995**, *30*, 1303.
[31] H. Ehring, B. U. R. Sundqvist. Excited-state relaxation processes of MALDI-matrices studied by luminescence spectroscopy. *Appl. Surf. Sci.* **1996**, *577*, 96.
[32] D. A. Alllwood, P. E. Dyer. Quantitative fluorescence measurements performed on typical matrix molecules in matrix-assisted laser desorption/ionization. *Chem. Phys.* **2000**, *261*, 457.
[33] H.-C. Lüdemann, R. W. Redmond, F. Hillenkamp. Singlet–singlet annihilation in ultraviolet matrix-assisted laser desorption/ionization studied by fluorescence spectroscopy. *R. Comunn. Mass Spectrom.* **2002**, *116*, 1287.

Supporting information

Additional supporting information may be found in the online version of this article at the publisher's web site.

